Published in final edited form as:
Neuron. 2010 October 6; 68(1): 73–86. doi:10.1016/j.neuron.2010.09.022.

Snapin-regulated late endosomal transport is critical for efficient autophagy-lysosomal function in neurons

Qian Cai[#], **Li Lu**[*], **Jin-Hua Tian**[*], **Yi-Bing Zhu**, **Haifa Qiao**, and **Zu-Hang Sheng**[#]
Synaptic Function Section, The Porter Neuroscience Research Center, National Institute of Neurological Disorders and Stroke, National Institutes of Health, Room 2B-215, 35 Convent Drive, Bethesda, Maryland 20892-3706, USA

Abstract

Neuron maintenance and survival require late endocytic transport from distal processes to the soma where lysosomes are predominantly localized. Here, we report a role for Snapin in attaching dynein to late endosomes through its intermediate chain (DIC). *Snapin* (−/−) neurons exhibit aberrant accumulation of immature lysosomes, clustering and impaired retrograde transport of late endosomes along processes, reduced lysosomal proteolysis due to impaired delivery of internalized proteins and hydrolase precursors from late endosomes to lysosomes, and impaired clearance of autolysosomes, combined with reduced neuron viability and neurodegeneration. The phenotypes are rescued by expressing the *snapin* transgene, but not the DIC-binding defective Snapin-L99K mutant. Snapin overexpression in wild-type neurons enhances late endocytic transport and lysosomal function, while expressing the mutant defective in Snapin-DIC coupling shows a dominant-negative effect. Altogether, our study highlights new mechanistic insights into how Snapin-DIC coordinates retrograde transport and late endosomal-lysosomal trafficking critical for autophagy-lysosomal function, thus neuronal homeostasis.

Keywords

lysosomes; autophagy; late endosome; late endocytic trafficking; retrograde transport; dynein

INTRODUCTION

Maintenance of neuronal morphology and function depends on efficient intracellular transport since the main synthetic and degradative compartments are located in the soma. Anterograde transport delivers newly synthesized organelles and macromolecules from the soma to distal processes and synapses while retrograde transport returns organelles in the endocytic and autophagic pathway to the soma (Goldstein and Yang, 2000; Hirokawa and Takemura, 2005). Late endocytic trafficking delivers target materials and internalized proteins to lysosomes for degradation (Luzio et al., 2007). The newly synthesized precursors of lysosomal hydrolases are transported from the trans-Golgi-network (TGN) through

[#]Correspondence should be addressed to Z.-H. Sheng or Q. Cai at Tel: 301-435-4596; Fax: 301-480-5763; shengz@ninds.nih.gov or caiq@ninds.nih.gov.
[*]These authors contributed equally to the paper.

COMPETING INTERESTS STATMENT
The authors declare no competing financial interests.

endosomes to acidic lysosomes for maturation (Ishidoh and Kominami, 2002). Thus, these two processes rely on the same trafficking pathway, which is crucial for the maturation and degradative capacity of the autophagy-lysosomal system. However, the cellular mechanisms regulating late endocytic trafficking pathway and its impact on lysosomal maturation and proteolysis in neurons are not fully understood.

Because lysosomes are predominantly localized in the soma and proximal region of neurons, dynein-dependent retrograde transport is critical for delivering late endosomal cargo from the cell periphery and distal processes to the soma bringing late endosomes and lysosomes into sufficient proximity to fuse with high efficiency. Perturbation of dynein-dynactin function results in the dispersion of late endocytic organelles to the cell periphery (Harada et al., 1998) and lysosomal proliferation (Chevalier-Larsen et al., 2008), impairs clearance of aggregate-prone proteins attributed to autophagy-lysosomal dysfunction (Ravikumar et al., 2005), and induces axonal degeneration (LaMonte et al., 2002; Hafezparast et al., 2003). However, the mechanisms coordinating late endocytic transport and lysosomal maturation, and therefore autophagy-lysosomal function in neurons, remain to be elucidated.

Snapin was first identified as a neuronal SNARE-binding protein (Ilardi et al., 1999) critical in priming large dense-core vesicles for fusion in chromaffin cells (Tian et al., 2005) and in facilitating synchronized fusion of synaptic vesicles (SVs) in neurons (Pan et al., 2009). In addition to its association with SVs, Snapin is present in membrane-associated fractions (Buxton et al., 2003) and co-purified with the biogenesis of lysosome-related organelle complex-1 (BLOC-1) (Starcevic and Dell'Angelica, 2004), highlighting its multivalent role in intracellular trafficking events. Because *snapin* (−/−) neurons display striking accumulation of late endocytic organelles, we investigated its role in late endocytic trafficking. Using biochemical, cellular and time-lapse imaging approaches in *snapin* mutant cortical neurons, combined with gene rescue experiments, we reveal a critical role for Snapin in coordinating late endocytic transport and lysosomal maturation—two dynamic cellular processes required for the proper function of the autophagy-lysosomal system in neurons. Such defects result in reduced neuron viability and neurodegeneration.

RESULTS

Deleting *snapin* Accumulates Immature Lysosomes and Impairs Lysosomal Function

We first examined the intracellular distribution of lysosomes in cultured cortical neurons from *snapin* (+/+) and (−/−) embryos with antibodies against MAP-2, a neuronal marker, and LAMP-1, a membrane protein associated with lysosomes. *Snapin* (−/−) neurons showed an increased mean intensity of LAMP-1 by 78% ($p<0.001$) relative to (+/+) neurons (Figure 1A). We then reintroduced the *snapin* transgene into the mutant neurons by transfection at 4 days *in vitro* (DIV4) and immunostained for LAMP-1 and MAP-2 at DIV8. Snapin gain-of-function reduced the mean intensity of LAMP-1 in the soma by 40% relative to neurons expressing GFP control (Figure 1B). Next, we examined the ultrastructural distribution of late endocytic compartments in cortical neurons using immuno-EM with an antibody against CI-MPR, a membrane protein preferentially located in late endosomes and immature, but not mature, lysosomes (Griffiths et al., 1988). CI-MPR-labeled organelles were intensely accumulated in *snapin* (−/−) neurons at DIV7 (Figures 1C and 1D). Average immunogold-labeled entities per soma section were 1.60 ± 0.25 for (+/+) and 6.25 ± 0.70 for (−/−) cortical culture (s.e.m., $p<0.01$), and average gold grains per soma section were 46.80 ± 6.72 for (+/+) and 141.58 ± 13.96 for (−/−) cortical culture ($p<0.01$). We also performed sequential immunoblots of cortical neuron lysates with various antibodies on the same blot membrane (Figure 1E). Increased intensities of both LAMP-1 and LAMP-2 were consistently observed in *snapin* (−/−) neurons, while expression of other organelle markers

including EEA1 (early endosomes), p115 (Golgi), and Calnexin (ER) exhibited no detectable change between *snapin* (+/+) and (−/−) neurons.

To further determine whether the accumulated LAMP-1-labeled organelles represent immature lysosomes, we first assessed the maturation of lysosomal hydrolases, which are normally transported from the TGN through late endosomes to lysosomes. Cathepsin D has been widely used as a reporter molecule for trafficking and maturation of lysosomal hydrolases; its mature light and heavy chains are produced by cleavage of its intermediate chain upon exposure to the acidic environment in mature lysosomes (Figure 1F). Any change in its mature forms reflects altered late endocytic trafficking or perturbed lysosomal maturation. Relative to their wild-type littermates, *snapin* deletion reduced mature heavy (30 kDa) and light (14 kDa) chains by 22.5±4.5% and 45.9±4.0%, respectively, and conversely, increased its intermediate forms (38–45 kDa) by 30.7±6.3% in mouse brain homogenates (Figure 1G).

To confirm defective maturation of lysosomal hydrolases, we alternatively labeled active cathepsin D in neurons by applying Bodipy-FL-pepstatin A, a fluorescence-tagged pepstatin A which binds specifically to the active site of cathepsin D in acidic lysosomes (Chen et al., 2000; Lee et al., 2010). While the majority of lysosomes were co-stained with Bodipy-FL-pepstatin A-labeled active cathepsin D in *snapin* (+/+) neurons, colocalization of active cathepsin D with LAMP-1 was substantially lower in *snapin* (−/−) neurons (Figure 1H). The normalized mean intensity of Bodipy-FL-pepstatin A in *snapin* (−/−) neurons was reduced by 46.1±2.6% (n=15, $p<0.001$) relative to (+/+) neurons (n=14), suggesting impaired maturation of cathepsin D, thus a reduced capacity of lysosomal degradation after *snapin* deletion.

We then examined whether *snapin* deficiency impacted cortical neuron viability in high-density culture. In neurons stained with neuron-specific class III β-tubulin antibody at DIV10, swelling puncta with diameters larger than processes were present along β-tubulin-labeled (−/−) but not (+/+) axonal processes (Figure S1A); similar structures were absent in MAP2-labeled *snapin* (−/−) dendrites from the same neurons, reflecting axonal swellings or axonal degeneration. *Snapin* (−/−) neurons maintained their growth density as well as (+/+) neurons until DIV8, after which the density was gradually reduced (Figure S1B). By DIV14, neuronal density was reduced to 44.7±5.3% relative to wild-type neurons, suggesting reduced viability in mature *snapin* (−/−) neurons. We next stained cortical culture through DIV0-14 with propidium iodide (PI), a vital dye labeling the nucleus in dying cells lacking an intact plasma membrane. Normalized number of PI-labeled dying cells increased by 7.5±1.8% (DIV10, $p<0.001$) and 7.0±1.9% (DIV14, $p=0.003$) in *snapin* (−/−) cortical culture relative to (+/+) culture, which is consistent with reduced neuronal growth density (Figure S1B). Furthermore, total and average dendrite length and total branch points in *snapin* (−/−) cortical neurons were reduced relative to their wild-type controls (Figures S1C and S1D). Homozygous *snapin* mice die perinatally (Tian et al., 2005). Thus, reduced viability, axonal swellings and developmental defects in *snapin*-deficient neurons may be attributable, at least in part, to the embryonic lethal phenotype of *snapin* null mice.

Deleting *snapin* Impairs Lysosomal Proteolysis due to Defective Late Endocytic Trafficking

We assessed the lysosomal degradation of epidermal growth factor (EGF) receptor (EGFR) in neurons. Endogenous EGFRs were primarily stained on the neuronal surface before EGF incubation. Following EGF treatment, EGFRs were internalized and clustered into large puncta. At 3h after EGF incubation, the normalized EGFR mean intensity reaches high levels with no detectable difference between *snapin* (+/+) and (−/−) neurons (Figure 2A and 2B). However, at 7h after EGF, a significant portion (35.82±2.8%, $p<0.001$) of internalized

EGFRs was degraded in (+/+) neurons while almost all EGFR puncta (93.59±5.86%, p=0.397) retained in *snapin* (−/−) neurons, suggesting a reduced capacity of lysosomal degradation after *snapin* deletion.

We next co-immunostained mouse embryonic fibroblasts (MEFs) and verified that *snapin* deletion resulted in aberrant accumulation of late endosomes/immature lysosomes co-labeled with LAMP-1 and CI-MPR (Figure S2A). In addition, the normalized mean intensity of acidic mature lysosomes labeled by the fluorescent pH indicator LysoSensor dye is substantially lower in *snapin* (−/−) MEFs relative to that in (+/+) cells (p<0.001)(Figure 2C), consistently indicating that LAMP-1-labeled organelles in both *snapin* (−/−) neurons and MEFs are primarily immature lysosomes.

Given that *snapin* (−/−) MEFs exhibit a similar accumulation of immature lysosomes, we next assessed late endocytic trafficking for the delivery and degradation of endocytosed proteins by performing three types of pulse-chase analyses using MEFs. MEFs have large flat cell bodies, allowing us to analyze late endocytic trafficking in greater detail. We first applied Alexa-488 conjugated EGF to monitor internalization and subsequent delivery to, and degradation in, lysosomes (Futter et al., 1996). There was no detectable difference in the normalized mean intensities of 488-EGF internalization between *snapin* (−/−) and (+/+) cells at a 10-min pulse (p=0.23) and a 30-min pulse (p=0.31). However, we observed an increased retention of internalized 488-EGF after a 3-hr chase in *snapin* (−/−) cells (Figure 2D). In contrast, the majority of internalized 488-EGF in (+/+) cells was degraded. Analysis of mean intensities revealed reduced degradation efficiency in (−/−) cells relative to controls (p=0.001) (Figure 2E). We immunostained MEFs following the pulse-chase. The retained EGF signals predominantly co-localized with CI-MPR (Figure S2B), but not with EEA-1 (Figures S2C), suggesting that EGF was retained in late endosomes. Western blot analysis further revealed that *snapin* deficiency significantly reduced EGFR degradation kinetics for up to 150 min compared with (+/+) MEFs (Figure S2D). As a control, there was no detectable change in transferrin uptake or recycling in the *snapin* (−/−) MEFs (Figure S2E), thus excluding the possibility of defective trafficking along the early endocytic pathway.

We performed a second pulse-chase assay using Alexa 488-dextran conjugates. Dextran moves along the same pathway as EGF following internalization but remains stable in lysosomes due to the lack of related hydrolases; altered dextran trafficking indicates impaired endosomal-lysosomal trafficking independent of lysosomal hydrolysis. MEFs were incubated with Alexa 488-dextran for 16 hr followed by a 4-hr chase to ensure that all internalized dextran was delivered to lysosomes. In *snapin* (+/+) MEFs, dextran co-localized with LAMP-I, but not with CI-MPR, confirming their targeting to mature lysosomes. In contrast, the internalized dextran in *snapin* (−/−) cells co-localized with CI-MPR (Figure 2F), but not with transferrin-labeled early/recycling endosomes (Figure S2F), indicating that dextran was retained in late endosomes rather than delivered to lysosomes.

To assess lysosomal degradative capacity at an ultrastructural level, we used electron microscopy to monitor the fate of internalized bovine serum albumin (BSA) conjugated with colloidal gold (BSA-gold). Internalized BSA-gold following fluid phase endocytosis and a pulse-chase protocol are flocculated within the late endocytic compartments after proteolytic degradation of BSA (Griffiths et al., 1988; Bright et al., 1997). Flocculation of gold particles in (+/+) MEFs was almost complete (99.09±0.91%, n=79 sections) after incubation with the conjugates for 4 hr at 37°C, followed by a 24-hr chase in conjugate-free medium (Figure 2G). However, in *snapin* (−/−) cells 38.24±1.10% (n=96 sections, p<0.01, Student's t test) of BSA-gold conjugates remained as discrete particles indicating impaired lysosomal degradative capacity. Thus, both defects in the transport of internalized proteins and hydrolase precursors from late endosomes to lysosomes could synergistically reduce

lysosomal degradative capacity, thereby contributing to the severe phenotypes observed in *snapin*-deficient cells.

Snapin Deficiency Reduces Clearance of Autolysosomes

Degradation of cytoplasmic constituents via autophagy primarily occurs upon fusion with lysosomes. Although autophagy is generally viewed as a stress-induced process, recent studies have highlighted its role during neuronal development and neurodegeneration (Komatsu et al., 2006; Hara et al., 2006; Fimia et al., 2007; Qu et al., 2007). We sought to determine whether Snapin was also necessary for proper autophagy function. Electron microscopy of the hippocampus from *snapin* (−/−) E18 brains demonstrated abnormal accumulation of autophagic vacuoles (Avd)(Figure 3A). Some of the Avd structures represent late autophagic vacuoles following fusion with lysosomes based on the morphologically defined features which: (1) contained partially degraded cytoplasmic material with higher electron density, and (2) were labeled by anti-LAMP1 immunogold (Figure 3B) (Kirkegaard et al., 2004). Avd accumulation may reflect increased formation of autophagosomes or reduced clearance of autolysosomes. The latter could be due to a reduction of lysosomal degradation. To differentiate between these two possibilities, we performed six types of experiments as recommended (Klionsky et al., 2008).

First, we analyzed autophagic marker LC3 in brain homogenates and MEF lysates. Deleting *snapin* substantially increased LC3, particularly LC3-II, under both starvation and nonstarvation conditions (Figure 3C). LC3-II is a lipidated form of LC3-I, which inserts into autophagic membranes (Kabeya et al., 2000) where it is eventually degraded by lysosomal hydrolases. Second, we examined autophagy markers p62/SQSTM1 (Bjørkøy et al., 2005) and LC3-II in non-starved cortical neuron lysates before and after treatment with lysosomal inhibitors (LIs) leupeptin and pepstatin A. Increased p62 and LC3-II were detected in *snapin* (−/−) neurons (Figure 3D). This phenotype mimics treatment with LIs in (+/+) neurons. In contrast, the same treatment of *snapin* (−/−) neurons failed to significantly increase LC3-II levels (p=0.07) (Figure 3E), reflecting reduced clearance of autolysosomes after *snapin* deletion. Third, we transfected GFP-LC3 in cortical neurons at DIV5 and treated with LIs at DIV6. GFP-LC3 appeared in vesicular structures in the soma of *snapin* (−/−) neurons but in a diffuse pattern in (+/+) neurons (Figure 3F). Deleting *snapin* significantly increased GFP-LC3 puncta (65.78 ± 14.50 per cell, p<0.01) relative to (+/+) neurons (11.06 ± 1.44 per cell) (Figure 3G). In (+/+) neurons, GFP-LC3 signals were recruited into vesicular structures in the presence of LIs, and the number of GFPLC3 puncta increased to 61.25 ± 8.73 per cell (p<0.01). In contrast, the same treatment of *snapin* (−/−) neurons with LIs failed to significantly increase LC3-II puncta (91.22 ± 12.85, p=0.19). Thus, our biochemical and cell imaging analysis suggest reduced clearance of autolysosomes after *snapin* deletion. Our interpretation is consistent with the current understanding of LC3 flux: If a gene mutation increases LC3-II levels in the absence of LIs, but there is no further increase in LIs, then there is likely a blockage of LC3-II degradation via autolysosomes (Klionsky et al., 2008).

Three more lines of evidence further support our notion. First, deleting *snapin* has no effect on the formation of autophagosomes in MEFs following starvation. Enhanced autophagy can be efficiently rescued by re-introducing *snapin* transgene (Figure S3A–D). Second, we immuno-isolated LAMP-1-labeled membranous organelles and detected increased p62 and LC3-II from the purified autolysosomal organelles in *snapin* (−/−) mice relative to wild-type littermates (Figure 3H). Third, we immunostained GFP-LC3-transfected MEFs with LAMP-1 and found that co-localization of GFP-LC3 with LAMP-1 in *snapin* (−/−) cells increased by 38.9±3.7% (p<0.001) relative to those of (+/+) cells in response to starvation (Figures S3E and S3F), suggesting that accumulated GFP-LC3 structures are largely composed of autolysosomes. Thus, our studies consistently support our notion that *snapin*

deficiency reduces clearance of autolysosomes due to impaired lysosomal degradative capacity.

Deleting *snapin* Impairs Retrograde Transport of Late Endosomes

Aberrant accumulation of immature lysosomes, impaired degradation of internalized proteins, and reduced clearance of autolysosomes in *snapin* (−/−) cells reflect altered late endosome-lysosome membrane trafficking. To elucidate the cellular mechanisms underlying the *snapin*-deficient phenotypes, we examined the distribution of late endocytic organelles in cortical neurons expressing late endosome marker YFP-Rab7. In (+/+) neurons, late endosomes appeared as small, fine vesicular structures evenly distributed along processes (Figure 4A). Surprisingly, late endosomes were clustered along (−/−) processes (Figure 4B). We then performed time-lapse imaging in live cortical neurons to assess the relative mobility of late endosomes along axons. Consistent with a previous report (Deinhardt et al., 2006), Rab7-labeled late endosomes exhibited active retrograde transport toward the soma in (+/+) neurons (Figure 4D, Video 1). In contrast, *snapin* deletion resulted in defective retrograde transport of the organelles and consequently increased their ratio in the stationary phase (Video 2). Re-introducing the *snapin* transgene into *snapin* (−/−) neurons not only rescued the defective retrograde transport, but also enhanced retrograde transport relative to (+/+) neurons (Figures 4C–E, Video 3). The transport defect was specific for late endocytic organelles as *snapin* deficiency had no observable effect on the distribution and axonal transport of mitochondria and early endosomes or distribution of ER and Golgi (Figure S4). Two-channel time-lapse imaging further demonstrated that in *snapin* (−/−) neurons, while late endosomes were predominantly stationary, mitochondria were dynamically mobile along the same axon (Video 4).

Snapin Is Required for Attaching Dynein to Late Endosomes

To examine whether Snapin associates with late endocytic compartments, we immuno-isolated Snapin or LAMP-1-associated membrane organelles using magnetic beads coated with antibodies against Snapin or LAMP-1. Snapin was detected together with Rab7, CI-MPR and LAMP-1 as well as late endocytic SNARE proteins including syntaxin7, syntaxin8 and Vti1b (Figures 5A and 5B). The relative purity was confirmed by the absence of markers for other membranous organelles including EEA1 (early endosomes), p115 (Golgi), and cytochrome *c* (mitochondria), suggesting selective association of Snapin with late endocytic membranes.

Immunoblot analysis of brain homogenates of *snapin* (+/+) and (−/−) littermates showed that *snapin* deletion resulted in no apparent changes in the expression of the dynein intermediate chain (DIC), light chain (LC8), dynactin $p150^{Glued}$, and KIF5B motor (Figure 5C). Immunoprecipitation of brain homogenates showed that deleting *snapin* has no observable effect on DIC interactions with its heavy chain (DHC) (Figure 5D) and dynactin $p150^{Glued}$ (data not shown). We then tested whether *snapin* deficiency impairs the attachment of the dynein motor to the late endocytic membranes. We immuno-isolated dynein motor-bound membrane organelles followed by immunoblotting. While an equal amount of DIC-associated membrane organelles were loaded, intensities of both LAMP-1 and LAMP-2 after *snapin* deletion were significantly reduced to 55.8±3.0% and 27.2±8.6%, respectively, relative to (+/+) control (Figure 5E), indicating reduced association of the dynein motor complex with late endocytic organelles in *snapin*-deficient neurons.

We next examined whether Snapin interacts with the dynein motor complex by applying a proteomic approach using GST-Snapin and rat brain homogenate. Coomassie blue staining of pulled-down proteins demonstrated one band at ~74 kDa (Figure 6A). Mass spectrometry of this protein band revealed a sequence consistent with rat DIC (sequence accession #

Q63100). To corroborate the mass spectrometry results, we repeated the pull-down study for Western blot with a DIC antibody, again verifying the 74-kDa band as DIC (Figure 6B). Dynactin, a known binding partner of DIC, was also pulled down together with DIC by GST-Snapin.

We further demonstrated a Snapin-DIC complex in neurons by immunoprecipitation. An anti-Snapin antibody co-precipitated DIC, but neither KIF5B nor Rab7, from mouse brain homogenates (Figure 6C). The efficacy of Snapin in its binding to DIC was also tested by co-immunoprecipitation using lysates from transfected COS-7 cells expressing both GFP-DIC and HA-Snapin. An anti-Snapin antibody co-immunoprecipitated GFP-DIC and HA-Snapin (Figure 6D). Conversely, reciprocal co-immunoprecipitation with an anti-GFP antibody pulled down both HA-Snapin and GFP-DIC (Figure 6E). Direct *in vitro* binding of GST-DIC to His-Snapin full-length but not to its N-terminal fragment was detected (Figure 6F). Truncated mutation analysis revealed the mouse DIC sequence between residues 108–268 as the Snapin-binding domain (Figure 6G). Thus, our immuno-isolation and proteomic approaches combined with GST pull-down, reciprocal immunoprecipitation and binding analysis suggest that Snapin acts as an adaptor linking dynein to the late endocytic membrane.

Snapin-DIC Interaction Is Crucial for Late Endocytic Transport and Membrane Trafficking

To provide a mechanistic link between dynein-driven retrograde transport of late endosomes and lysosomal biology, we generated Snapin mutants defective in DIC-binding by replacing a single hydrophobic residue with lysine within the carboxyl-terminal coiled-coil domain. Snapin-V92K and -L99K mutants substantially reduced their binding to GST-DIC (Figure 7A). Expressing Snapin-L99K in *snapin* (−/−) neurons failed to rescue the defective retrograde transport of late endosomes along axons (Figures 7B and 7D) and failed to correct the abnormal accumulation of lysosomes in (−/−) neurons (Figure 7E). Furthermore, expressing Snapin-L99K in (+/+) neurons clustered late endosomes along processes and reduced their axonal mobility (Figures 7C and 7D). These phenotypes mimic what were found in *snapin* (−/−) neurons (Figure 4), suggesting a dominant-negative effect by disrupting Snapin-DIC interaction.

To mechanically link the dominant-negative effect of Snapin-L99K on the retrograde transport to lysosomal degradative capacity, we conducted an EGF pulse-chase assay in *snapin* (+/+) MEFs. While there was no detectable change after a 30-min pulse period, internalized Alexa-555-EGF in cells expressing Snapin-L99K displayed increased retention after a 3-hr chase (Figure S5A). In contrast, the majority of internalized 555-EGF in cells expressing the GFP control was degraded. Quantification of normalized mean intensities revealed an average 40% reduction in lysosomal degradation efficiency in the cells expressing Snapin-L99K relative to GFP controls (p=0.012) (Figure S5B).

To exclude the possibility that impaired SV priming and fusion in *snapin*-deficient neurons is a side effect of defective late endocytic trafficking, we evaluated the modes of action of Snapin-L99K and -C66A mutants. The latter is a Snapin mutant defective in binding to synaptotagmin-I and SNAP-25 and is unable to rescue impaired SV priming and fusion (Pan et al., 2009). Re-introducing Snapin-C66A not only rescued the impaired transport of late endosomes in *snapin* (−/−) neurons (Figure 7D) but also effectively reversed the aberrant accumulation of immature lysosomes in (−/−) MEFs (Figures S5C and S5D). Conversely, expressing Snapin-L99K effectively rescued impaired SV release (Figures S5E and S5F). Thus, mutual rescue effects of these two mutants suggest that Snapin plays independent roles in SV priming/fusion and late endocytic transport via distinct modes of action.

Snapin/Dynein-Mediated Transport Enhances Late Endosomal-Lysosomal Trafficking

Elevated Snapin expression not only rescued the retrograde transport of late endosomes in *snapin* (−/−) neurons but also enhanced the transport rate in (+/+) neurons (Figure 4), indicating that Snapin is a rate-limiting factor in the regulation of late endosomal transport. We next examined the morphology of neuronal lysosomes following elevated Snapin expression. While GFP-LAMP-1-labeled lysosomes appeared as vesicular structures predominantly localized in the soma of *snapin* (+/+) cortical neurons, elevated Snapin expression increased the number of tubular lysosomes (>3 μm) (Figures 8A and 8B). Formation of tubular lysosomes was inhibited following expression of Snapin-L99K or the Snapin-binding domain of the DIC (108–268) transgene, further indicating a critical role of Snapin-DIC interaction in regulating lysosomal biology. Since lysosomal membrane extension depends on motor proteins and microtubules (Swanson et al., 1992), our findings highlight the possibility that Snapin facilitates the formation of tubular lysosomal structures by providing the motion force through Snapin-DIC interaction, thus accelerating late endosomal-lysosomal trafficking.

To more directly assess the role of the Snapin-DIC interaction, we labeled lysosomes with GFP-LAMP-1 and marked late endosomes with Alexa-546-dextran by short pulse-chase (1.5 hrs). Relative to neurons expressing HA, elevated Snapin expression induced more late endosomes (red) incorporated into lysosomes (green) to form vesicular (arrowheads) or tubular (arrows) endolysosomes (yellow) in the soma (Fig. 8C). In contrast, neurons expressing Snapin-L99K or DIC (108–268) transgene displayed reduced formation of endolysosomes. Quantitative analysis revealed a substantial increase in the fluorescent intensity ratio of GFP-LAMP-1/dextran-546 in neurons overexpressing Snapin (1.85±0.16, $p<0.01$) relative to that of control neurons expressing HA (0.99±0.05). However, disrupting the Snapin-DIC interaction with Snapin-L99K or DIC (108–268) transgene reduced the ratio by 0.45±0.03 or 0.44±0.04, respectively ($p<0.01$) (Figure 8D). Thus, Snapin/dynein-mediated retrograde transport enhances late endosomal-lysosomal membrane trafficking.

We then monitored Snapin-induced dynamic formation of tubular lysosomes in live COS-7 cells following labeling of late endosomes with YFP-Rab7 and long pulse-chase loading (20-hr) of lysosomes with Rhodamine-dextran (Bright et al., 2005; Lakadamyali et al., 2006). Time-lapse images frequently captured the formation of highly dynamic long tubular organelles labeled by both YFP-Rab7 and Rhodamine-dextran in the cells over-expressing Snapin—a phenotype observed at a much lower frequency in control cells (Figure 8E, Videos 5 and 6). Such dynamic events resulted in content mixing (yellow) between the late endosomes (green) and lysosomes (red), some of which occurred within a 30-sec time frame. The fast influx of late endocytic content into the tubular hybrid compartment was viewed more clearly by displaying fluorescence intensity in scaled pseudocolor. Elevated Snapin expression increased the number and average length of tubular lysosomes (Figure 8F), mimicking a previously reported phenotype induced by facilitating late endocytic membrane trafficking (Bright et al., 2005).

DISCUSSION

Lysosomal hydrolase precursors and internalized materials must be delivered from late endosomes to acidic lysosomes for proper lysosomal maturation and degradation. Our study reveals that Snapin acts as an adaptor linking late endosomes to the dynein motor and thus plays a key role in coordinating two dynamic processes: (1) dynein-driven retrograde transport of late endosomes; and (2) late endosomal-lysosomal membrane trafficking and lysosomal maturation. Coordinating these two processes is particularly challenging for neurons because most acidic mature lysosomes are generated in the soma and proximal axon (Overly and Hollenbeck, 1996). Snapin-dynein-mediated retrograde transport is essential for

the delivery of late endosomal cargo from distal processes to the soma, where late endosomes and lysosomes would be in sufficient proximity for membrane trafficking with higher efficiency by the motor-driven force (Figure S6). Such a mechanism enables neurons to maintain efficient degradation capacity and cellular homeostasis via the autophagy-lysosomal pathway.

In *snapin*-deficient neurons, the association of late endosomes with dynein was significantly impaired resulting in the following three major defects: (1) fewer late endosomes were transported from the cell periphery or distal processes toward the soma resulting in their clustering within neuronal processes; (2) efficacy of late endocytic membrane trafficking was altered, reducing delivery of internalized materials to lysosomes for efficient degradation and impairing trafficking of hydrolase precursors or intermediates through late endosomes to acidic lysosomes for maturation, resulting in proliferation of immature lysosomes; and (3) turnover of autolysosomes was impaired. All these phenotypes could effectively be rescued by the Snapin wild-type transgene but not by the DIC-binding defective Snapin-L99K mutant. In addition, elevated Snapin expression selectively enhances retrograde transport of late endosomes to a greater extent than in wild-type neurons. Furthermore, Snapin overexpression provides greater motion force to produce elongated lysosomes in proximal processes and soma and facilitates the formation of tubular lysosomes. In contrast, formation of tubular lysosomes is blocked after expression of Snapin-L99K or DIC (108–268). These data provide a mechanistic link between dynein-driven retrograde transport and late endocytic trafficking / lysosomal maturation, thus demonstrating a new cellular pathway in regulating lysosomal function. It was recently reported that protolysosomal tubules extruded from autolysosomes mature into functional lysosomes (Yu et al., 2010). Thus, formation of tubular lysosomes may reflect accelerated recycling of the lysosomal membrane following Snapin-enhanced late endocytic transport and lysosomal proteolysis.

Clearance of autolysosomes depends on proper lysosomal function. *Snapin* deficiency leads to buildup of autolysosomes. Re-introducing *snapin* into (−/−) cells rescued the phenotype, indicating its critical role in maintaining a balance between the rate of autophagic sequestration and completion of degradation. Thus, impaired autophagy in *snapin*-deficient mice is attributable to defective late endocytic trafficking and lysosomal dysfunction, which is consistent with recent findings that aberrant late endosomal/lysosomal structure or trafficking was associated with impaired autophagosome degradation (Zhong et al., 2009).

Cytoplasmic dynein, a principal motor driving retrograde transport, is composed of heavy chains (DHC), intermediate chains (DIC), light intermediates (DLIC) and light chains (DLC). Cargos attach to the dynein motor with a degree of specificity, and the dynein-cargo linkage via an adaptor may be a general mechanism in neurons. Bassoon functions as a cargo adaptor for dynein via an interaction with DLC and is essential for retrograde transport of Piccoloo-Bassoon transport vesicles and their distribution among synapses (Fejtova et al., 2009). Snapin contributes to late endocytic transport by binding to DIC and attaching the dynein motor to late endocytic membranes. Snapin co-exists with the dynein complex in the purified late endocytic compartments and interacts directly with DIC, thus providing a physical link between Snapin and the dynein motor. Deleting *snapin* resulted in reduced association of the dynein motor to late endosomes. Expressing Snapin-L99K mutant defective in DIC-binding failed to rescue the defective late endocytic trafficking and impaired lysosomal function. Moreover, this mutant exhibits dominant-negative effects when expressed in wild-type cells, thus providing compelling evidence that the Snapin-DIC interaction is critical for dynein-driven retrograde transport of late endosomes and for efficient endosome-lyososmal trafficking.

Dynein mutation or autophagy dysfunction leads to prominent neurodegeneration (Hafezparast et al., 2003; Hara et al., 2006; Komatsu et al., 2006). Reduced neuron viability, defective dendritic development and axonal swellings found in *snapin* (−/−) cortical neurons provide direct and compelling evidence that Snapin-mediated and dynein-driven retrograde transport of late endosomes is crucial for neuronal development and survival by maintaining autophagy-lysosomal function and cellular homeostasis. Alternatively, dynein-driven retrograde transport supplies the soma with survival signals in the form of "signaling endosomes" carrying the neurotrophin-Trk complexes (Deinhardt et al., 2006; Cosker et al., 2008; Perlson et al., 2009). Late endosome-lysosome compartments may also regulate neurite outgrowth by adding new membrane (Sann et al., 2009) or lysosomal exocytosis, thus changing neuronal viability and dendritic morphology. It was also reported that Snapin-cypin interaction impacts dendritic morphology through changing microtubule stability (Chen et al., 2005).

At least a dozen Snapin-binding proteins have been reported including SNAP-25, synaptotagmin I, cypin, and dysbindin (Buxton et al., 2003; Tian et al., 2005; Chen et al., 2005; Talbot et al., 2006), highlighting its multivalent role in a variety of membrane trafficking systems. Although Snapin binds to endosomal syntaxin 8 (Lu et al., 2009), it is unlikely that it regulates lysosomal function directly via SNARE-fusion machinery. First, Snapin-DIC interaction can easily be detected by Coomassie blue staining (Fig. 6A) and by applying a proteomic approach, while binding of Snapin to syntaxin 8 is relatively weaker. Second, the interactions among the endosomal SNARE proteins in *snapin*-null mice are not significantly impaired (data not shown). Third, DIC-binding defective Snapin-L99K plays a dominant-negative role in retrograde transport and lysosomal biology, but has an unaffected binding to syntaxin 8 and other known Snapin-binding proteins including SNAP-25, synaptotagmin-1, dysbindin, and cypin (Figure S5G). Fourth, expressing Snapin-L99K or DIC (108–268) transgene in (+/+) neurons exhibits a similar dominant-negative effect on the formation of tubular lysosomes and late endosome-lysosome trafficking. However, future investigation into whether Snapin targets to late endosomes via binding to the endocytic SNAREs is required.

Snapin was co-purified with BLOC-1 (Starcevic and Dell'Angelica, 2004). Mutation of BLOC-1 genes in mice results in Hermansky-Pudlak syndrome-like phenotypes characterized by defects in cell type-specific lysosome-related organelles (LROs) including melanosomes and platelet-dense granules. However, these mice are fully viable and demonstrate no defects in the morphology, trafficking and function of late endosomes or lysosomes (Falcón-Pérez et al., 2005). Given the distinct *snapin* mouse phenotypes, Snapin likely plays a more specific role in regulating late endocytic transport and lysosomal maturation. *Snapin*-null mice exhibit neonatal death, and mutant neurons display axonal swelling reflecting more critical roles rather than the cell type-specific role of BLOC-1. Our study may provide a clue as to whether Snapin also links the dynein motor to LROs.

In summary, our study provides a mechanistic link between late endocytic transport and lysosomal function. Such a mechanism is critical for quality control of intracellular components and cellular homeostasis, and is thus essential for neuronal survival and development. Snapin as a key component of the late endocytic transport machinery provides a molecular target to regulate autophagy-lysosomal function. The *snapin* KO mouse represents one of the few genetic models displaying such striking phenotypes and provides us with a unique genetic tool to characterize the role of late endocytic transport in the clearance of aggregated protein and dysfunctional organelles during neurodegeneration.

EXPERIMENTAL PROCEDURES

Materials and detailed methods can be found in the Supplemental Information.

EGFR and EGF Degradation Assay

For the EGFR degradation assay, cortical neurons were starved in culture medium in the absence of B27 supplement for 15 min and then treated for 30 min at 4°C with culture medium containing EGF (5μg/ml), followed by incubation at 37°C with medium in the absence of EGF for various times before fixation and immunostaining with antibodies against MAP2 and EGFR. For the EGF degradation assay, MEFs were starved overnight in serum-free medium (SFM: DMEM containing 10 mM HEPES and 0.2% BSA) followed by incubation with 0.5 μg/ml Alexa Fluor 488 or 555-conjugated EGF (Invitrogen) at 37°C for 1 hr. After 3 washes with ice-cold SFM, the cells were again incubated with feeding medium (DMEM containing 10% FBS) at 37°C for various lengths of time before fixation for confocal imaging.

Immunoisolation of Late Endocytic Organelles

Liver or brain tissue from E17-18 *snapin* WT or KO embryo was homogenized in the buffer (10 mM HEPES [pH 7.4], 1 mM EDTA, 0.25 M sucrose, and protease inhibitors) and centrifuged at 750×g for 10 min, after which the supernatant collected. The pellet was suspended in homogenization buffer and re-centrifuged at 750×g for 10 min. The combined first and second supernatants were centrifuged at 3,500×g for 10 min and at 23,000×g for 20 min. The pellet was then suspended in homogenization buffer and subjected to immuno-isolation with tosylated Dynabeads (Invitrogen) as previously described (Tian et al., 2005).

Labeling of Lysosomes with Internalized Dextran

Cells were loaded with 0.5 mg/ml Alexa Fluor 488-conjugated Dextran (Invitrogen) at 37°C for 16 hr followed by incubation in conjugate-free medium for 4 hr. The cells were then incubated with 25 μg/ml Alexa Fluor 555-conjugated transferrin and processed for imaging or fixed with 4% formaldehyde and stained with antibodies to LAMP-1 or CI-MPR. Time-lapse images were captured in a series of 100 frames and quantified by measuring the number and maximal length of tubular lysosomes at every 10th frame.

Autophagy Assay

Cultured cortical neurons were treated with 20 μM lysosomal inhibitors (Leupeptin and Pepstatin A) and harvested after a 24-hr incubation. For the analysis of GFP-LC3 puncta, the cells were transfected with GFP-LC3 for 20 hr followed by starvation in HBSS, or maintained in DMEM with 10% FBS (complete medium) for 3 hr.

Measurement of Neuronal Density and Cell Viability

For determining neuron density, the number of the MAP2-stained cortical neurons were counted in 10 randomly selected image fields from each coverslip with a 20×objective from DIV0 through DIV14. Data were averaged from three independent experiments. For cell viability assay, cortical neurons were treated with 10 μg/ml Propidium iodide (PI) at 37°C for 30 min, followed by imaging in Tyrode's solution.

Labeling of Active Cathepsin D with Bodipy-FL-pepstatin A

Neurons were incubated with 1 μM Bodipy-FL-pepstatin A in Neurobasal medium for 1 h at 37°C followed by fixation and immunostaining with antibodies against MAP2 and LAMP-1.

Labeling of Acidic Organelles

1 μM LysoSensor Green was added to *snapin* (+/+) and (−/−) MEFs in the growth medium and incubated at 37°C for 30 min before imaging under confocal microscope.

Kymographs

Kymographs were made using extra plug-ins for ImageJ (NIH). The height of the kymographs represents recording time (495 sec unless otherwise noted), while the width represents the length (μm) of the axon imaged.

Image Acquisition

Confocal images were obtained using a Zeiss LSM 510 oil immersion 40×or 63×objective with sequential-acquisition setting. For fluorescent quantification, images were acquired using the same settings below saturation at a resolution of 1,024×1,024 pixels (12 bit). Morphometric measurements were performed using Image-Pro Plus (Media Cybernetics) or Metamorph (Universal Imaging) or NIH ImageJ.

Statistical Analysis

Images are representative of > 10 cells from at least 3 repeats. All immunoblots are representative of at least 3 experiments. Statistical analyses were performed using unpaired Student's *t*-test and are presented as mean ± SEM.

Supplementary Material

Refer to Web version on PubMed Central for supplementary material.

Abbreviation

CI-MPR	cation-independent mannose-6-phosphate receptors
DIV	days *in vitro*
DIC	dynein intermediate chain
MAP-2	microtubule-associated proteins-2
LAMP-1	lysosome-associated membrane protein-1
MEFs	mouse embryonic fibroblasts
EGF	epidermal growth factor

Acknowledgments

We thank R. Youle, H. Arnheiter and members of the Sheng lab for helpful discussions; D. Glazer-Schoenberg, M. Davis and J. Tokita for editing; X. Zhuang, B. Firestein, P. D. Stahl, W. Li, N. Raben for reagents; NINDS Facility for Electron Microscopy, DNA Sequencing, and Protein Sequencing. L Lu and Y-B. Zhu are graduate students of the NIH-Shanghai Jiao-Tong University Joint Ph.D. Program. This work was supported by the Intramural Research Program of NINDS, NIH (Z-H. S.) and the NIH Pathway to Independence Award K99 (Q.C.).

Animal care and use was carried out in accordance with NIH guidelines and was approved by the NIH, NINDS/NIDCD Animal Care and Use Committee.

References

Bjørkøy G, Lamark T, Brech A, Outzen H, Perander M, Overvatn A, Stenmark H, Johansen T. p62/SQSTM1 forms protein aggregates degraded by autophagy and has a protective effect on huntingtin-induced cell death. J. Cell Biol. 2005; 171:603–614. [PubMed: 16286508]

Bright NA, Reaves BJ, Mullock BM, Luzio JP. Dense core lysosomes can fuse with late endosomes and are re-formed from the resultant hybrid organelles. J. Cell Sci. 1997; 110:2027–2040. [PubMed: 9378754]

Bright NA, Gratian MJ, Luzio JP. Endocytic delivery to lysosomes mediated by concurrent fusion and kissing events in living cells. Curr. Biol. 2005; 15:360–365. [PubMed: 15723798]

Buxton P, Zhang XM, Walsh B, Sriratana A, Schenberg I, Manickam E, Rowe T. Identification and characterization of Snapin as a ubiquitously expressed SNARE-binding protein that interacts with SNAP23 in non-neuronal cells. Biochem. J. 2003; 375:433–440. [PubMed: 12877659]

Chen CS, Chen WN, Zhou M, Arttamangkul S, Haugland RP. Probing the cathepsin D using a BODIPY FL-pepstatin A: applications in fluorescence polarization and microscopy. J Biochem. Biophys. Methods. 2000; 42:137–151. [PubMed: 10737220]

Chen M, Lucas KG, Akum BF, Balasingam G, Stawicki TM, Provost JM, Riefler GM, Jörnsten RJ, Firestein BL. A novel role for snapin in dendrite patterning: interaction with cypin. Mol. Biol. Cell. 2005; 16:5103–5114. [PubMed: 16120643]

Chevalier-Larsen ES, Wallace KE, Pennise CR, Holzbaur EL. Lysosomal proliferation and distal degeneration in motor neurons expressing the G59S mutation in the p150Glued subunit of dynactin. Hum. Mol. Genet. 2008; 17:1946–1955. [PubMed: 18364389]

Cosker KE, Courchesne SL, Segal RA. Action in the axon: generation and transport of signaling endosomes. Curr. Opin. Neurobiol. 2008; 18:270–275. [PubMed: 18778772]

Deinhardt K, Salinas S, Verastegui C, Watson R, Worth D, Hanrahan S, Bucci C, Schiavo G. Rab5 and Rab7 control endocytic sorting along the axonal retrograde transport pathway. Neuron. 2006; 52:293–305. [PubMed: 17046692]

Falcón-Pérez JM, Nazarian R, Sabatti C, Dell'Angelica EC. Distribution and dynamics of Lamp1-containing endocytic organelles in fibroblasts deficient in BLOC-3. J. Cell Sci. 2005; 18:5243–5555.

Fejtova A, Davydova D, Bischof F, Lazarevic V, Altrock WD, Romorini S, Schöne C, Zuschratter W, Kreutz MR, Garner CC, Ziv NE, Gundelfinger ED. Dynein light chain regulates axonal trafficking and synaptic levels of Bassoon. J Cell Biol. 2009; 185:341–355. [PubMed: 19380881]

Fimia GM, et al. Ambra1 regulates autophagy and development of the nervous system. Nature. 2007; 447:1121–1125. [PubMed: 17589504]

Futter CE, Pearse A, Hewlett LJ, Hopkins CR. Multivesicular endosomes containing internalized EGF-EGF receptor complexes mature and then directly with lysosomes. J. Cell Biol. 1996; 132:1011–1023. [PubMed: 8601581]

Goldstein LS, Yang Z. Microtubule-based transport systems in neurons: the roles of kinesins and dyneins. Annu. Rev. Neurosci. 2000; 23:39–71. [PubMed: 10845058]

Griffiths G, Hoflack B, Simons K, Mellman I, Kornfeld S. The mannose 6-phosphate receptor and the biogenesis of lysosomes. Cell. 1988; 52:329–341. [PubMed: 2964276]

Hafezparast M, et al. Mutations in dynein link motor neuron degeneration to defects in retrograde transport. Science. 2003; 300:808–812. [PubMed: 12730604]

Hara T, Nakamura K, Matsui M, Yamamoto A, Nakahara Y, Suzuki-Migishima R, Yokoyama M, Mishima K, Saito I, Okano H, Mizushima N. Suppression of basal autophagy in neural cells causes neurodegenerative disease in mice. Nature. 2006; 441:885–889. [PubMed: 16625204]

Harada A, Takei Y, Kanai Y, Tanaka Y, Nonaka S, Hirokawa N. Golgi vesiculation and lysosome dispersion in cells lacking cytoplasmic dynein. J Cell Biol. 1998; 141:51–59. [PubMed: 9531547]

Hirokawa N, Takemura R. Molecular motors and mechanisms of directional transport in neurons. Nat Rev Neurosci. 2005; 6:201–214. [PubMed: 15711600]

Ichimura Y, Kominami E, Tanaka K, Komatsu M. Selective turnover of p62/A170/SQSTM1 by autophagy. Autophagy. 2008; 4:1063–1066. [PubMed: 18776737]

Ilardi JM, Mochida S, Sheng ZH. Snapin: a SNARE-associated protein implicated in synaptic transmission. Nat. Neurosci. 1999; 2:119–124. [PubMed: 10195194]

Ishidoh K, Kominami E. Processing and activation of lysosomal proteinases. Biol. Chem. 2002; 383:1827–1831. [PubMed: 12553719]

Kabeya Y, Mizushima N, Ueno T, Yamamoto A, Kirisako T, Noda T, Kominami E, Ohsumi Y, Yoshimori T. LC3, a mammalian homologue of yeast Apg8p, is localized in autophagosome membranes after processing. EMBO J. 19:5720–5728. [PubMed: 11060023]

Kirkegaard K, Taylor MP, Jackson WT. Cellular autophagy: surrender, avoidance and subversion by microorganisms. Nat. Rev. Microbiol. 2004; 2:301–314. [PubMed: 15031729]

Klionsky DJ, et al. Guidelines for the use and interpretation of assays for monitoring autophagy in higher eukaryotes. Autophagy. 2008; 4:151–175. [PubMed: 18188003]

Komatsu M, Waguri S, Chiba T, Murata S, Iwata J, Tanida I, Ueno T, Koike M, Uchiyama Y, Kominami E, Tanaka K. Loss of autophagy in the central nervous system causes neurodegeneration in mice. Nature. 2006; 441:880–884. [PubMed: 16625205]

Lakadamyali M, Rust MJ, Zhuang X. Ligands for clathrin-mediated endocytosis are differentially sorted into distinct populations of early endosomes. Cell. 2006; 124:997–1009. [PubMed: 16530046]

LaMonte BH, Wallace KE, Holloway BA, Shelly SS, Ascaño J, Tokito M, Van Winkle. T, Howland DS, Holzbaur EL. Disruption of dynein/dynactin inhibits axonal transport in motor neurons causing late-onset progressive degeneration. Neuron. 2002; 34:715–727. [PubMed: 12062019]

Lee JH, et al. Lysosomal proteolysis and autophagy require presenilin 1 and are disrupted by Alzheimer-related PS1 mutations. Cell. 2010; 141:1146–1158. [PubMed: 20541250]

Lu L, Cai Q, Tian JH, Sheng ZH. Snapin associates with late endocytic compartments and interacts with late endosomal SNAREs. Biosci. Rep. 2009; 29:261–269. [PubMed: 19335339]

Luzio JP, Pryor PR, Bright NA. Lysosomes: fusion and function. Nat. Rev. Mol. Cell Biol. 2007; 8:622–632. [PubMed: 17637737]

Overly CC, Hollenbeck PJ. Dynamic organization of endocytic pathways in axons of cultured sympathetic neurons. J. Neurosci. 1996; 16:6056–6064. [PubMed: 8815888]

Pan PY, Tian JH, Sheng ZH. Snapin facilitates the synchronization of synaptic vesicle fusion. Neuron. 2009; 61:412–424. [PubMed: 19217378]

Perlson E, Jeong GB, Ross JL, Dixit R, Wallace KE, Kalb RG, Holzbaur EL. A switch in retrograde signaling from survival to stress in rapid-onset neurodegeneration. J Neurosci. 2009; 29:9903–9917. [PubMed: 19657041]

Qu X, Zou Z, Sun Q, Luby-Phelps K, Cheng P, Hogan RN, Gilpin C, Levine B. Autophagy gene-dependent clearance of apoptotic cells during embryonic development. Cell. 2007; 128:931–946. [PubMed: 17350577]

Ravikumar B, Acevedo-Arozena A, Imarisio S, Berger Z, Vacher C, O'Kane CJ, Brown SD, Rubinsztein DC. Dynein mutations impair autophagic clearance of aggregate-prone proteins. Nat. Genet. 2005; 37:771–776. [PubMed: 15980862]

Sann S, Wang Z, Brown H, Jin Y. Roles of endosomal trafficking in neurite outgrowth and guidance. Trends Cell Biol. 2009; 19:317–324. [PubMed: 19540123]

Starcevic M, Dell'Angelica EC. Identification of snapin and three novel proteins (BLOS1, BLOS2, and BLOS3/reduced pigmentation) as subunits of biogenesis of lysosome-related organelles complex-1 (BLOC-1). J. Biol. Chem. 2004; 279:28393–28401. [PubMed: 15102850]

Swanson JA, Locke A, Ansel P, Hollenbeck PJ. Radial movement of lysosomes along microtubules in permeabilized macrophages. J. Cell Sci. 1992; 103:201–209. [PubMed: 1429905]

Talbot K, Cho DS, Ong WY, Benson MA, Han LY, Kazi HA, Kamins J, Hahn CG, Blake DJ, Arnold SE. Dysbindin-1 is a synaptic and microtubular protein that binds brain snapin. Hum. Mol. Genet. 2006; 15:3041–3054. [PubMed: 16980328]

Tian JH, Wu ZX, Unzicker M, Lu L, Cai Q, Li C, Schirra C, Matti U, Stevens D, Deng C, Rettig J, Sheng ZH. The role of Snapin in neurosecretion: snapin knock-out mice exhibit impaired calcium-dependent exocytosis of large dense-core vesicles in chromaffin cells. J. Neurosci. 2005; 25:10546–10555. [PubMed: 16280592]

Yu L, McPhee CK, Zheng L, Mardones GA, Rong Y, Peng J, Mi N, Zhao Y, Liu Z, Wan F, Hailey DW, Oorschot V, Klumperman J, Baehrecke EH, Lenardo MJ. Termination of autophagy and reformation of lysosomes regulated by mTOR. Nature. 2010; 465:942–946. [PubMed: 20526321]

Zhong Y, Wang QJ, Li X, Yan Y, Backer JM, Chait BT, Heintz N, Yue Z. Distinct regulation of autophagic activity by Atg14L and Rubicon associated with Beclin 1-phosphatidylinositol-3-kinase complex. Nat Cell Biol. 2009; 11:468–476. [PubMed: 19270693]

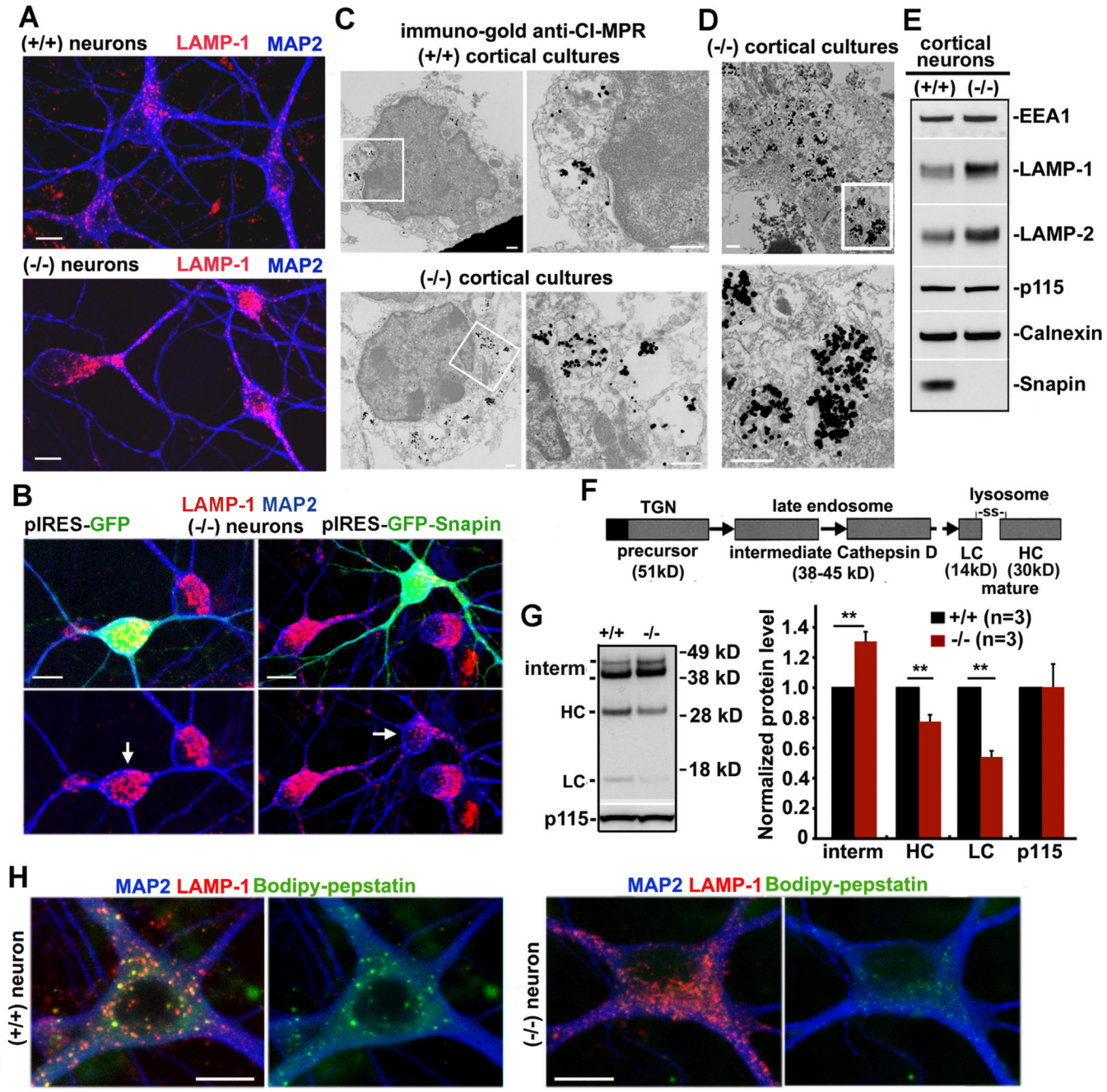

Figure 1. Aberrant Accumulation of Immature Lysosomes in *snapin* (−/−) Neurons

(A) Cortical neurons from *snapin* (+/+) and (−/−) embryos were co-immunostained at DIV7 with antibodies against MAP2 and LAMP-1.

(B) Re-introducing *snapin* rescued accumulated LAMP-1-labeled organelles in *snapin* (−/−) neurons. Neurons were transfected with pIRES-GFP-Snapin or pIRES-GFP as a control at DIV4 and co-immunostained for LAMP-1 and MAP2 at DIV8. Arrows indicate transfected neurons.

(C, D) Immature lysosomes in cortical neuron cultures. Late endosomes/immature lysosomes labeled by anti-CI-MPR-immunogold were clustered in the soma (C) and

processes (D) of *snapin* (−/−) neurons at DIV7. Right panels (C) and lower panel (D) are close-up views of the boxed regions.

(E) Increased LAMP-1 and LAMP-2 in *snapin* (−/−) cortical neurons. 40-μg lysates were sequentially detected in the same membrane with antibodies including markers for early endosomes (EEA1), Golgi (p115), and ER (Calnexin).

(F) Schematic diagram of cathepsin D maturation during trafficking from TGN through late endosomes to lysosomes.

(G) Impaired maturation of cathepsin D in *snapin* (−/−) mouse brain. 40-μg brain homogenates from E18 embryos were immunoblotted with antibodies against cathepsin D and p115. Percent change in the intermediate chains (interm) and mature forms of the heavy (HC) and light chain (LC) of cathepsin D was normalized against that of wild-type littermates. ** $p<0.01$. Error bars: s.e.m. Student's *t* test.

(H) Reduced cathepsin D activity in *snapin* (−/−) cortical neurons. Neurons were loaded with Bodipy-FL-pepstatin A followed by co-staining with antibodies against MAP2 and LAMP-1. Note that reduced active cathepsin D signals (green) were co-localized with lysosomes (red) in (−/−) cells.

Scale bars in panels C and D: 500 nm; in other panels: 10 μm. (also see Figure S1).

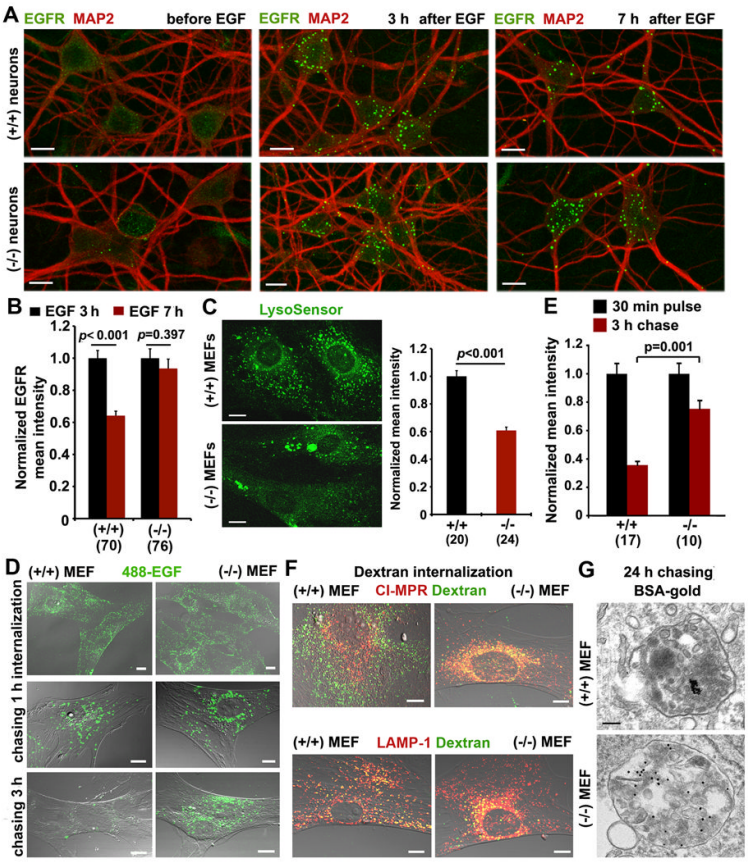

Figure 2. *Snapin* Deletion Impairs Late Endocytic Trafficking and Lysosomal Degradation

(A, B) Reduced degradation of internalized EGFR in *snapin* (−/−) cortical neurons. Cortical neurons were co-immunostained with MAP2 and EGFR before or 3 h or 7 h after EGF incubation (A). The EGFR mean intensity was normalized against MAP2 from the same neurons and expressed as ratios relative to the mean intensity at 3 h EGF incubation (B).

(C) Reduced acidic lysosomes in *snapin* (−/−) MEFs labeled by fluorescence pH indicator LysoSensor (green). Mean intensity (right panel) of LysoSensor fluorescence in *snapin* (−/−) MEFs was normalized to those in (+/+) controls.

(D, E) Pulse-chase assays showing impaired degradation of Alexa-488-EGF in *snapin* (−/−) MEFs. The mean intensity of 488-EGF after a 3-hr chase was normalized against that after the 30-min pulse (E).

(F) Deleting *snapin* impaired delivery of internalized dextran to lysosomes. Note that most dextran signals were retained in CI-MPR-labeled late endosomes.

(G) Electron microscopy showing impaired degradation of BSA-gold in *snapin* (−/−) MEFs. Gold particles were flocculated in the late endocytic compartments of *snapin* (+/+) cells due to BSA degradation, while BSA-gold conjugates remained discrete within the organelles of the *snapin* (−/−) MEFs.

The total number of cells quantified is indicated in parentheses under bar graphs. Scale bars in G: 100 nm; in other panels: 10 μm. Error bars: s.e.m. Student's *t* test, (also see Figure S2).

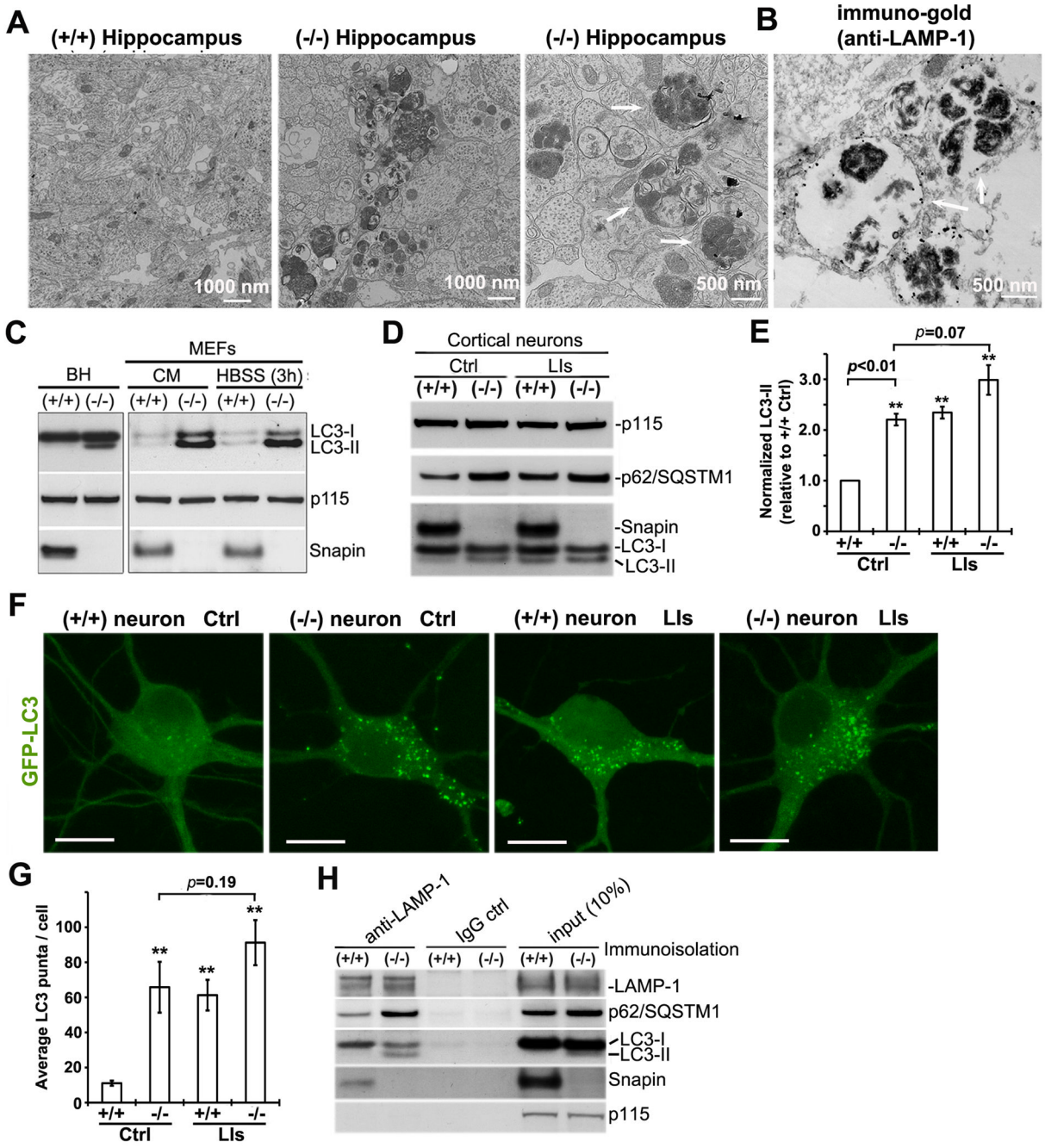

Figure 3. Snapin Deficiency Reduces Autolysosome Clearance

(A) Electron micrographs of hippocampi from *snapin* (+/+) and (−/−) embryos (E18). Clustered Avd-like structures with higher electron density (arrows) were consistently found in *snapin* (−/−) hippocampus. Images were selected near perinuclear regions.

(B) Immunogold EM of cultured *snapin* (−/−) cortical neurons (DIV7) revealed LAMP-1-labeled structures similar to Avds in *snapin* (−/−) mouse hippocampi and suggestive of autolysosomes.

(C) Enhanced LC3-II in *snapin* (−/−) brain homogenates (BH, 40 μg) and MEF lysates (20 μg) cultured in complete medium (CM) or starvation medium (HBSS) for 3 hr.

(D, E) Biochemical analysis showing reduced clearance of autolysosome substrates p62 and LC3-II in *snapin* (−/−) cortical neurons. Neurons were treated with DMSO or the lysosomal inhibitors (LIs) leupeptin and pepstatin A (20 μM each) for 24 hrs. 40-μg lysates were sequentially immunobloted with antibodies against p62, LC3, Snapin and p115. The intensity of LC3-II bands (gels=4) was normalized to p115 and expressed as a ratio relative to (+/+) Ctrl (**: $p<0.01$) (E). Treating (−/−) neurons with LIs failed to significantly increase LC3-II level ($p=0.07$).

(F, G) Cell biological analysis showing reduced turnover of GFP-LC3-labeled organelles in *snapin* (−/−) cortical neurons. Neurons were transfected with GFP-LC3 at DIV5 and treated with DMSO or LIs (leupeptin and pepstatin A, 20 μM each) at DIV6 for 24 hrs. GFP-LC3 signals were recruited into vesicular structures in *snapin* (+/+) neurons following LI treatment. Treating *snapin* (−/−) neurons with LIs failed to significantly increase LC3-II puncta ($p=0.19$) (G).

(H) Increased p62 and LC3-II in autolysosomes from *snapin* (−/−) brains. LAMP-1-associated membranous organelles were immuno-isolated from light membrane fractions of *snapin* (+/+) and (−/−) mouse brains with Dyna magnetic beads coated with an anti-LAMP-1 antibody. Relative purity was assessed by measuring LAMP-1 and p115 levels. Scale bars in F: 10 μm, (also see Figure S3).

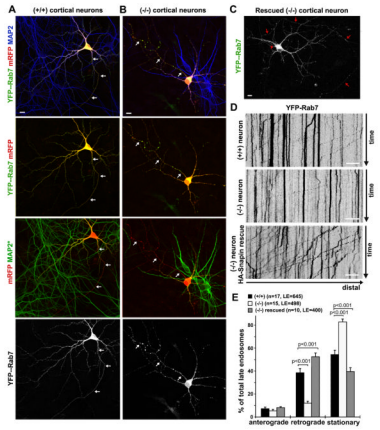

Figure 4. Impaired Retrograde Transport of Late Endosomes in *snapin* (−/−) Cortical Neurons

(A–C) Representative images showing distribution patterns of Rab7-labeled late endosomes in *snapin* (+/+) (A), (−/−) (B), and rescued cortical neurons (C). Neurons were co-transfected with mRFP and YFP-Rab7 at DIV6 followed by immunostaining with an anti-MAP2 antibody at DIV7. Late endosomes in *snapin* (−/−) neurons appear as large clusters along processes, while in (+/+) and rescued neurons they display as a much smaller punctate pattern. Arrows indicate axons. MAP*: blue MAP2 signal was converted to green for better color comparison.

(D) Representative kymographs showing the mobility of axonal late endosomes during 12-min recordings in *snapin* (+/+), (−/−) and rescued neurons. Vertical lines represent stationary organelles; oblique lines or curves to the right represent anterograde movements and lines to the left indicate retrograde transport. Re-introducing HA-Snapin into (−/−) neurons recruits stationary organelles into the retrograde mobile pool.

(E) Relative mobility of axonal late endosomes in *snapin* (+/+), (−/−) and rescued neurons. Data were quantified from the total number of axonal late endosomes (LE) in neurons (n) from >3 experiments, as indicated in parentheses. Scale bars: 10 μm. Error bars: s.e.m. Student's *t* test, (also see Figure S4 and Videos 1–4).

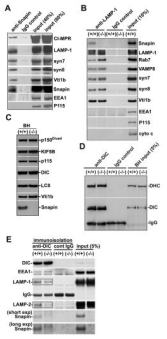

Figure 5. Snapin Is Required for Tethering Dynein to the Late Endocytic Membrane

(A, B) Snapin associates with late endocytic compartments. Snapin- or LAMP-1-associated organelles were immuno-isolated from light membrane fractions of *snapin* (+/+) and (−/−) mouse livers with Dyna magnetic beads coated with either anti-Snapin (A) or anti-LAMP-1 (B) antibody, or normal IgG as a control. Bead-bound organelles were resolved by PAGE and sequentially detected with antibodies on the same membranes after stripping between applications of each antibody.

(C, D) Deleting *snapin* has no observable effect on dynein motor expression in brain homogenates (BH) (50 μg) (C) or on assembly of DIC into the dynein heavy chain (DHC) (D). DIC-DHC complex was immunoprecipitated with a DIC antibody from 500 μg BH of *snapin* (+/+) and (−/−) mice.

(E) Deleting *snapin* reduces association of dynein with late endocytic organelles. Dynein-associated membranous organelles were immuno-isolated from light membrane fractions with anti-DIC-coated Dyna magnetic beads. Reduced LAMP-1 and LAMP-2 (in boxes) were associated with dynein-bound organelles from *snapin* (−/−) mice.

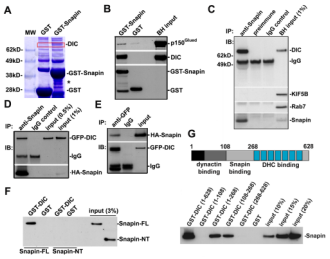

Figure 6. Snapin Directly Interacts with Dynein DIC

(A) Coomassie Blue staining of GST-Snapin pull-down from rat brain homogenates. Mass spectrometry of the 74-kDa band (in red box) matches the rat DIC sequence. (*indicates degradation of GST-Snapin).

(B) GST-Snapin pulls down dynein and dynactin from rat brain homogenates (BH).

(C) Immunoprecipitation of Snapin with DIC from BH with an anti-Snapin antibody, normal IgG or pre-immune serum as controls, followed by sequential blotting with antibodies as indicated.

(D, E) Snapin-DIC complex was immunoprecipitated by antibodies against either Snapin (D) or GFP (E) from COS cells expressing HA-Snapin and GFP-DIC.

(F) Binding of GST-DIC to His-Snapin full-length (FL) but not to its N-terminal half (NT).

(G) Snapin-binding sequence. DIC has an N-terminal coiled-coil domain required for binding to $p150^{Glued}$, a middle Snapin-binding domain, and a C-terminal half containing 7 WD repeats involved in DHC binding.

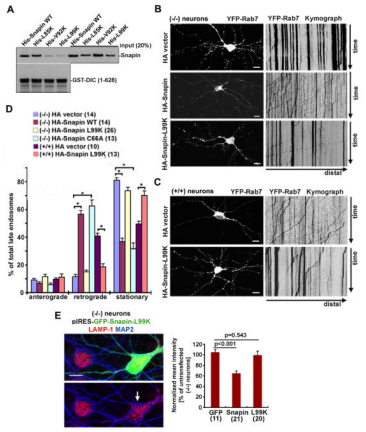

Figure 7. DIC–Binding Defective Snapin Mutant Fails to Rescue Late Endosomal Transport and Lysosomal Biology

(A) GST-DIC pull-down showing defective binding to Snapin-V92K and L99K mutants.

(B) Representative images showing distribution of YFP-Rab7-labeled late endosomes (left) and kymographs showing their axonal mobility (right) in *snapin* (−/−) neurons co-transfected with YFP-Rab7 and HA-Snapin, HA-Snapin-L99K, or HA vector control.

(C) Representative images and kymographs showing a dominant-negative effect of Snapin-L99K on axonal retrograde transport of late endosomes in (+/+) neurons.

(D) Relative mobility of axonal late endosomes in (+/+) or (−/−) neurons expressing Snapin or Snapin-L99K or those expressing the Snapin-C66A, a defective binding mutant for synaptotagmin I and SNAP-25.

(E) Expressing Snapin-L99K in *snapin* (−/−) cortical neurons failed to rescue accumulated immature lysosomes. Neurons were transfected with pIRES-GFP-Snapin-L99K followed by immunostaining with antibodies against LAMP-1 and MAP2. Arrow indicates transfected neuron. The total number of neurons examined is indicated in parentheses from >3 experiments. Scale bars: 10 μm. Error bars: s.e.m. *:$p<0.001$. Student's *t* test, (also see Figure S5).

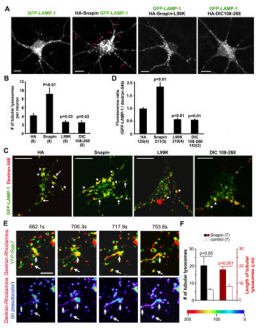

Figure 8. Snapin Enhances Formation of Tubular Lysosomes or Endolysosomes by Interacting with DIC

(A, B) Snapin, but neither its L99K mutant nor the Snapin-binding domain of the DIC108–268 transgene, enhances formation of tubular lysosomes (indicated by red arrows) in cortical neurons (A). Number of tubular lysosomes per neuron (B) was counted in neurons co-expressing GFP-LAMP-1 with HA-Snapin, HA-Snapin-L99K, HA-DIC108–268 or HA vector control.

(C, D) Snapin, but neither its L99K mutant nor DIC108–268, facilitates formation of endolysosomes in the soma of cortical neurons (C). Lysosomes were labeled by GFP-LAMP-1 and late endosomes were marked by a short-chase loading of dextran-546. Average fluorescence ratios of GFP-LAMP-1 / dextran-546 were calculated from individual vesicular (arrowheads) or tubular (arrows) endolysosomes (D).

(E, F) Snapin expression in COS cells enhances late endocytic membrane trafficking. Representative time-lapse images demonstrate dynamic tubular lysosome formation via fusion between late endosomes (green) and lysosomes (red) within the indicated time period in cells expressing HA-Snapin (E). Rhodamine-Dextran fluorescence levels are also shown in scaled pseudocolor. Arrows indicate tubulation or fusion events. Note that the minus-end is pointed toward the lower left side. The number and average length of tubular lysosomes in cells expressing Snapin were quantified relative to controls (F). Scale Bars in A and C: 10 μm; in E: 5 μm. Student's *t* test, (also see Figure S6 and Videos 5 and 6).